GLOBALNA ANALIZA ATMOSFERSKIH REFRAKCIJSKIH PROFILOV IZ PREKRIVANJ RADIJSKIH SIGNALOV COMSIC GPS

GLOBAL ANALYSIS OF ATMOSPHERIC REFRACTIVITY PROFILES FROM COSMIC GPS RADIO OCCULTATION SOUNDINGS

Shaoqi Gong, Cunjie Zhang, Geshi Tang, Yehui Zhang, Jing Han

UDK: 528.28:629.052
Klasifikacija prispevka po COBISS.SI: 1.01
Prispelo: 24. 9. 2019
Sprejeto: 8. 6. 2020

DOI: 10.15292/geodetski-vestnik.2020.02.227-240
SCIENTIFIC ARTICLE
Received: 24. 9. 2019
Accepted: 8. 6. 2020

IZVLEČEK

Atmosferska refrakcija je odvisna od temperature, tlaka in vodne pare. Iz GNSS ocenjena refrakcija ima dovolj dobro vertikalno ločljivost in točnost, da jo lahko vključimo v numerične modele napovedi vremena ter uporabimo v meteoroloških in klimatskih raziskavah. V študiji smo ovrednotili razlike med modelom refrakcije, pridobljenim iz sistema COSMIC, in izračuni iz podatkov vertikalne radiosondaže, in sicer za različne višine, geografske širine in letne čase. Analizirali smo časovne in globalne prostorske porazdelitvene vzorce atmosferske refrakcije na podlagi podatkov COSMIC za atmosferske ravni, kjer zračni tlak znaša 925 hPa in 300 hPa. Rezultati so pokazali, da je ocenjena refrakcija v splošnem podobna oceni iz podatkov radiosond. Razlika se značilno manjša z višino, ko je v troposferi tlak nad 300 hPa, nad tropopavzo pa so razlike komaj še zaznavne. Izrazite razlike med oceno refrakcije iz podatkov COSMOS oziroma podatkov, pridobljenih z radiosondami, se kažejo s spreminjanjem geografske širine in z letnim časom. Globalna refrakcija COSMIC na višini, kjer je tlak 825 hPa, je najvišja v tropskem pasu ter se manjša proti severni in južni hemisferi. V atmosferi na višini, kjer je tlak 300 hPa, je z refrakcijo ravno nasprotno. Anomalije refrakcije glede na srednjo letno vrednost so večje v januarju in juliju, manjše pa v aprilu in oktobru.

KLJUČNE BESEDE

atmosferska refrakcija, COSMIC, GPS-radarska prekrivanja, radiosonda, časovna in prostorska porazdelitev

ABSTRACT

Atmospheric refractivity is a function of temperature, pressure and water vapor. The refractivity retrieved from the GNSS radio occultation soundings has fine vertical resolution and high accuracy, so it can be used to improve the accuracy of numerical weather prediction models and in climate and meteorological research. This study evaluates differences of refractivity from the COSMIC against radiosondes (RS) at different atmospheric levels, latitudes and seasons. Then temporal and global spatial distribution patterns of the COSMIC refractivity are analyzed at the atmospheric levels of 925 and 300 hPa. The results indicate that the COSMIC and RS refractivities are in generally good agreement. The differences between COSMIC and RS refractivity decrease with increasing height in the troposphere above 300 hPa, and the differences are very small above the tropopause. The COSMIC-RS differences exhibit distinct latitudinal and seasonal variation. The global COSMIC refractivity at 925 hPa is the highest in the tropics, and it decreases with increasing latitude in the NH and SH. However, the refractivity at the atmospheric levels of 300 hPa is just the opposite. Refractivity anomalies relative to the annual mean values in January and July are significant, whereas the differences are not as large in the transitional seasons of April and October.

KEY WORDS

atmospheric refractivity, COSMIC, GPS radio occultation, radiosonde, temporal and spatial distribution

1 INTRODUCTION

When an electromagnetic wave travels through the atmosphere, the wave is bent (refracted), and the signal is delayed due to the vertical gradient of density in the atmosphere; this phenomenon has a crucially important effect on radar detection, satellite navigation and radio communication systems on Earth (Karimian et al., 2011; Tang et al., 2019). Corrections for radio refraction can improve the accuracy of radar measurements and the performance of communication systems (Jiang and Wang, 2001). The refractivity is dependent on the air temperature, pressure and humidity (Smith and Weintraub, 1953). Hence, the atmospheric refractivity is an essential variable in numerical weather prediction data assimilation (Kuo et al., 2000).

The atmospheric refractivity can be retrieved by radar measurements (Zhang et al., 2015; Lòpez and Río, 2018), radiosonde soundings (Kapungu et al., 1981; Adeyemi, 2004), ground-based GPS receivers (Bevis et al., 1992; Lowry et al., 2002; Liao et al., 2016), and low Earth orbit (LEO) satellite GNSS RO soundings (Ao et al., 2003; Cucurull et al., 2006). Weather radar has a suitable vertical and horizontal resolution for measuring refractivity, but there are few stations globally. A radiosonde (RS) is a conventional instrument for observing atmospheric profiles; it has a long history and near-global coverage over land, but are usually launched only twice a day. Bevis et al. (1992) first presented an approach to retrieve atmospheric water vapor based on ground-based GPS receivers. Lowry et al. (2002) estimated the refractivity structure by establishing a model between ground-based GPS excess phase path and the refractivity. Ground-based GPS receivers have very high temporal resolution with a 5-min interval, however, these receivers are limited to land.

Although radio occultation (RO) was recognized as an important potential technology to characterize the atmosphere as early as the 1960s (Phinney and Anderson, 1968; Fjeldbo and Eshleman, 1969), due to the high cost of space-borne transmitters and insufficient accuracy of satellite positioning in the early period, the first LEO satellite (MicroLab-1) with a GPS RO receiver was not launched until 3 April 1995 (Ware et al., 1996). These first RO soundings exhibited fine vertical resolution and high accuracy (within 1 K) for the air temperature and geopotential height of 10–20 m (Poli et al., 2002). Subsequently, many RO missions were successively launched. The German Challenging Minisatellite Payload (CHAMP) and the Argentinean Satélite de Aplicaciones Cientificas-C (SAC-C) were launched in 2000, and approximately 350-500 RO soundings per day were obtained from the two satellites (Wickert et al., 2001; Hajj et al., 2004). The joint US-Taiwan mission FORMOSAT-3/COSMIC (Formosa Satellite Mission-3/Constellation Observing System for Meteorology, Ionosphere and Climate; hereafter COSMIC) was launched on 14 April 2006 and was just recently (1 May 2020) decommissioned. The mission consisted of a constellation of six identical small satellites and provided about 2000 RO soundings per day from 2006 to 2015 distributed around the globe in near-real-time (Rocken et al., 2000; Anthes, 2011; Ho et al., 2019).

Since RO soundings have many advantages including low cost, high accuracy, high vertical resolution, no need for calibration, long-term stability, unaffected by cloud cover or rainfall, and global coverage (Anthes et al., 2000; Anthes, 2011), they have received increased attention for monitoring the climate and predicting the weather. Various types of data such as bending angle, refractivity, temperature, and precipitable water vapor, which are retrieved from RO soundings, are also used increasingly in

climate and meteorological studies (Liu and Zou, 2003; Huang et al., 2005; Wee et al., 2008). Kuo et al. (2000) concluded that the bending angles and refractivity were the two best candidates for assimilation and it was demonstrated that the use of these parameters had a significant positive impact on global and regional weather prediction. Cucurull et al. (2006) assessed the impact of simulated COSMIC GPS RO refractivity on operational weather analysis in the Antarctic. Chen et al. (2009) developed a nonlocal observation operator to assimilate COSMIC RO refractivity in the Weather Research and Forecasting Model (WRF) and the three-dimensional variational data assimilation (3DVAR) system. Ha et al. (2014) assimilated GPS RO soundings from COSMIC and CHAMP in the Weather Research and Forecast (WRF) model to analyze and forecast a heavy rainfall event over the Korean Peninsula in October 2006.

Many studies on the accuracy assessment of RO soundings both COSMIC and other missions have been carried out. Kuo et al. (2004) evaluated the accuracy of refractivity from CHAMP RO soundings. Lohmann (2007) analyzed the errors characteristics from SAC-C RO measurements. Poli et al (2009) assessed the quality of bending angle, refractivity, refractivity lapse rate and temperature from COSMIC RO soundings. Xu et al. (2009) compared the refractivity differences between COSMIC and radiosondes in different altitudes, latitudes and seasons. Anthes (2011) reviewed studies that showed that RO could provide accurate and precise atmospheric profiles of electron density, refractivity, temperature and water vapor by multi-satellite missions CHAMP, SAC-C, GRACE, METOP-A, TerraSAR-X and COSMIC. Chen et al. (2011) estimated the observational errors of refractivity and linear excess phase from COSMIC GPS RO data. Wang et al. (2013) assessed the accuracy of COSMIC RO retrieval products including temperature, specific humidity, water vapor pressure and refractivity by comparing with global radiosonde data. Schreiner et al. (2020) evaluated signal-to-noise ratio of COSMIC-2 soundings from GPS and GLONASS signals and estimated the differences of bending angle and refractivity between COSMIC-2 and other data sets.

Since COSMIC RO soundings are of high vertical resolution and accuracy, they can be used to evaluate the quality of measurements from other instruments. He et al. (2009) assessed the performance of radiosonde for temperature measurements using COSMIC RO data. Ho et al. (2010, 2017) evaluated the systematic biases of water vapor and temperature from radiosonde measurements using COSMIC RO soundings. However, there have been very few studies of COSMIC refractivity compared to radiosonde refractivity on a global basis.

In this study, COSMIC RO refractivities were first matched with RS data in the range of 2 h and 300 km. Subsequently, daily refractivity at different atmospheric levels in January, April, July and October 2014 were compared with corresponding radiosonde data. Then the differences between COSMIC and RS refractivity at different heights, latitudes and seasons were determined. Finally, the temporal and spatial distribution patterns of COSMIC refractivity in the globe were considered. This paper is organized as follows: Section 2 presents the data used in the analysis and the preprocessing methods; Section 3 discusses the COSMIC-RS refractivity differences at different heights, latitudes and seasons, and the temporal and spatial distribution patterns of COSMIC refractivity in the globe; Section 4 provides the summary and conclusions.

2 DATA AND METHODS

2.1 Refractivity profiles retrieved from COSMIC GPS RO soundings

RO soundings are obtained by a GPS receiver on the COSMIC satellites when the radio signal from a GPS satellite traverses Earth's atmosphere. The basic parameters of the sounding are the amplitude and phase of the carrier signals. After the clock biases of the GPS transmitter and COSMIC GPS receiver have been calibrated, the Doppler frequency shift of the carrier signal can be computed by the amplitude and phase (Hajj et al., 2002). The bending angle α, which is defined as the angle between the incident and outgoing directions of the GPS radio signal and is a function of the impact parameter a, is determined from the Doppler frequency shift, the position and the velocity of the spacecraft (Rocken et al., 1997; Liao et al., 2016). After the ionospheric effects have been removed, the bending angle is converted to the refractive index n(r) using the Abel integral algorithm under the assumption of local spherical symmetry (Fjeldbo et al., 1971):

$$n(r) = \exp[\frac{1}{\pi}\int_x^\infty \frac{\alpha(a)}{\sqrt{a^2 - x^2}} da] \tag{1}$$

Since n is typically close to 1 in the atmosphere, it is more convenient to use the refractivity N instead. Hence, the refractivity N can be calculated by the refractive index n,

$$N(r) = (n - 1) \times 10^6 \tag{2}$$

In this study, the global atmospheric refractivity data were downloaded from the COSMIC Data Analysis and Archive Center (https://cdaac-www.cosmic.ucar.edu/cdaac/products.html#cosmic). The data were post-processing level-2 wetPrf files including the profiles of pressure, height, refractivity, temperature and water vapor pressure with 100 m vertical resolution; the data were the result of one-dimensional variational analysis using low-resolution reanalysis data of the European Centre for Medium-Range Weather Forecasts (ECMWF) (Wang et al., 2013; Hande et al. 2015).

2.2 Refractivity profiles retrieved from radiosonde soundings

Since the global radiosonde network was established in the early 1940s, radiosondes have been the principal instruments used for observing the troposphere and lower stratosphere. There are more than 1000 radiosonde stations distributed worldwide (Ware et al., 1996; Wang et al., 2005). Radiosonde balloons are launched twice a day at 00:00 and 12:00 UTC to observe the atmospheric profiles. The observations include geopotential height, air pressure, air temperature, relative humidity, wind speed and wind direction at standard levels (1000, 925, 850, 700, 500, 400,300, 250, 200, 150 and 100 hPa). Under ideal conditions and after careful calibration, radiosondes provide data with an accuracy of about ±0.5ºC for temperature and a few percent for relative humidity (Zhai and Eskridge, 1997; Ware et al., 1996). Hence, radiosondes have been regarded as a benchmark to calibrate satellite-based remote sensing data and validate satellite retrieval results (Wang et al., 2005). In this study, the refractivity profiles calculated from RS soundings are compared to the COSMIC refractivity profiles. The radiosonde refractivity at each standard atmospheric level is calculated using data for air temperature, air pressure and water vapor partial pressure and the Smith and Weintraub (1953) equation:

$$N = 77.6\frac{P}{T} + 3.73\times10^5 \frac{e}{T^2} \tag{3}$$

where N is the refractivity in N-units, T is the temperature in Kelvin, P and e are pressure and water vapor partial pressure in hPa, respectively. The global RS daily data were obtained from the Meteorological Observatory at Nanjing University of Information Science and Technology, China.

2.3 Co-location of COSMIC RO refractivity with radiosonde data

The positions of all the COSMIC occultation points change daily, whereas those of the global radiosonde stations are relatively fixed, except for small changes due to balloon drift. In order to compare the COSMIC refractivity data and the radiosonde data, the observation times and positions for two datasets at each point must be close. Similar to previous studies, the COSMIC RO refractivity data were matched to the radiosonde data within 300 km and 2 h (Kuo et al., 2005; Hayashi et al., 2009; Xu et al., 2009). The processing consisted of the following steps: first, a vector file was generated for the longitude and latitude of the global radiosonde stations and a circular buffer with a radius of 300 km around each radiosonde station was created; second, the vector file of the COSMIC RO refractivity was generated using the geographical coordinates of all occultation points. Then, all the daily COSMIC vector files were respectively integrated with the radiosonde buffer area file using an intersection operation, and the attributes of the points were joined to create a spatial match of both datasets. These procedures are quickly implemented through the batch module in the Geographic Information System software ArcGIS 10.5. Third, a time difference of ±2 hours was considered for the match between the COSMIC RO refractivity and the radiosonde data. For example, for 2 January 2014, there were 123 co-located occultation points (Figure 1). Each COSMIC refractivity profile had 400 levels with a 100-m interval, whereas the radiosonde data had a dozen levels in the vertical profile. The refractivity values at standard atmospheric levels of 1000, 925, 850, 700, 500, 400, 300, 250, 200, 150, and 100 hPa, which correspond to approximate atmospheric heights of 0.13, 0.78, 1.49, 3.07, 5.68, 7.32, 9.33, 10.53, 11.96, 13.80 and 16.36 km respectively, were selected for the comparison. There were possible outliers in the matched pairs at different atmospheric levels and when the outliers were excluded from the matched pairs, the number of the matched pairs was different at each atmospheric level.

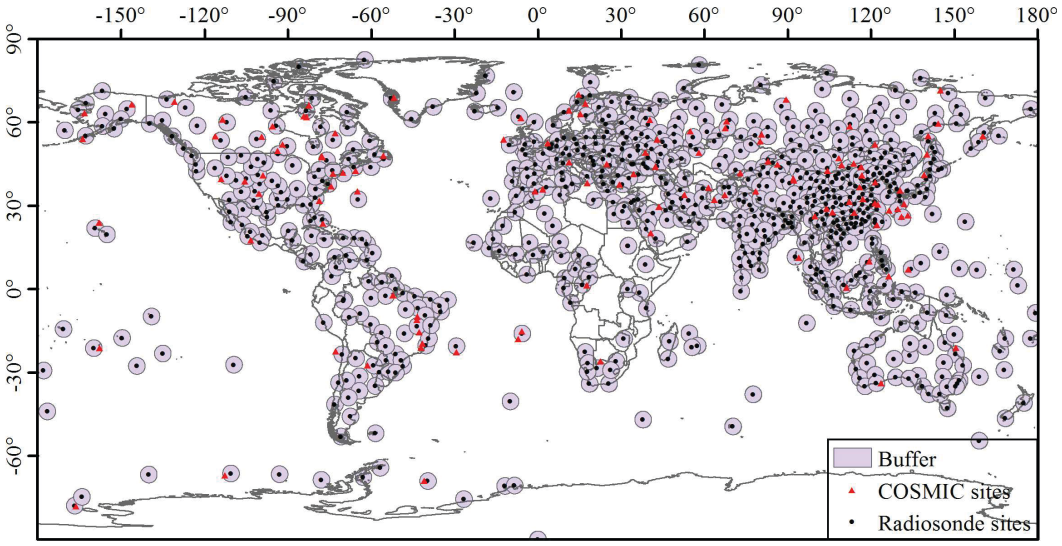

Figure 1: Co-location of COSMIC RO refractivity with radiosonde data on 2 January 2014.

3 RESULTS AND DISCUSSION

3.1 Comparison of COSMIC and radiosonde refractivity

Vertical profiles of the mean and standard deviation of the COSMIC refractivities are shown in Figure 2*a*. The mean and standard deviations of the refractivity decrease with height. The relationship between atmospheric refractivity and the height can be expressed by an exponential model (Bean and Thayer, 1959).

The COSMIC refractivity at each atmospheric level was compared with that of the radiosonde and scatter plots of the COSMIC vs radiosonde refractivity were created for each level (Figure 2*b*–*l*). The mean bias (MB), root mean square difference (RMSD) and mean absolute percentage difference (MAPD) were calculated. When the MB is close to 0, the RMSD and MAPD are small, and the points are distributed near the 1:1 line, the fitted line is very close to the 1:1 line in the scatter plot, indicating good agreement between the COSMIC and RS refractivity. The differences are caused by observational errors in both the COSMIC and radiosonde data. Additionally, they are also associated with the sampling differences due to separation in time and space (Sun et al. 2010; Gilpin et al, 2018) and the representativeness errors (Staten and Reichler, 2009; Anthes and Rieckh, 2018).

Figure 2*b*–*l* shows the scatter plots of the refractivity between COSMIC and radiosonde at different atmospheric levels, the number of the matched pairs is 4409 at 1000 hPa, increases to the maximum of 9136 at 500 hPa, and then decreases gradually to 6236 at 100 hPa. As seen in the scatter plots, most of the matched data points are distributed near the 1:1 line (dashed lines), and the correlation coefficients range from 0.752 to 0.966; indicating that there is generally good agreement between the COSMIC and the radiosonde refractivities. The correlation coefficients are relatively low (about 0.75) at the levels of 1000–750 hPa, they increase to 0.85 at 500 hPa and are higher than 0.90above 400 hPa. The RMSD decreases with height. The MAPD is 4.29% near the ground at 1000 hPa, reaches a minimum of 0.72% at the top of the troposphere at 300 hPa, and then increases slightly to 0.89% in the lower stratosphere at 100 hPa. Although the COSMIC and radiosonde refractivity differences decline with an increase in the height, the MAPD increases slightly above the tropopause, consistent with the fact that the percentage errors of RO generally increase with height throughout the stratosphere (as shown, for example, in Schreiner et al., 2020). The mean bias (MB) is -3.82 N-units near the ground at 1000 hPa, decreases to –0.05 N-units with increasing height, and then stabilizes at about –0.05 N-units at the subsequent levels. The MB is negative at all atmospheric levels, which indicates that the COSMIC refractivity is slightly lower than the radiosonde refractivity. As shown in the scatter plots, the discrepancy between the fitted line and the 1 : 1 line in the scatter plots is relatively large at the atmospheric levels of 1000–500 hPa, but there is less discrepancy at atmospheric levels below 400 hPa, and the two lines are nearly coincident at the levels of 150 and 100 hPa. These results show that the differences of the COSMIC-RS refractivity are a little larger below 500 hPa; this is mainly attributed to relatively larger errors of COSMIC refractivity due to the influence of the atmospheric water vapor causing strong refractivity gradients (Sokolovskiy, 2003) and the low signal-to-noise ratio in the lower troposphere. These results are consistent with the previous validations for RO data (Kuo et al., 2005; Schreiner et al., 2007; Anthes et al., 2008). On the whole, the differences of COSMIC-RS refractivity decrease as the atmospheric height increased in the range of 1000–100 hPa.

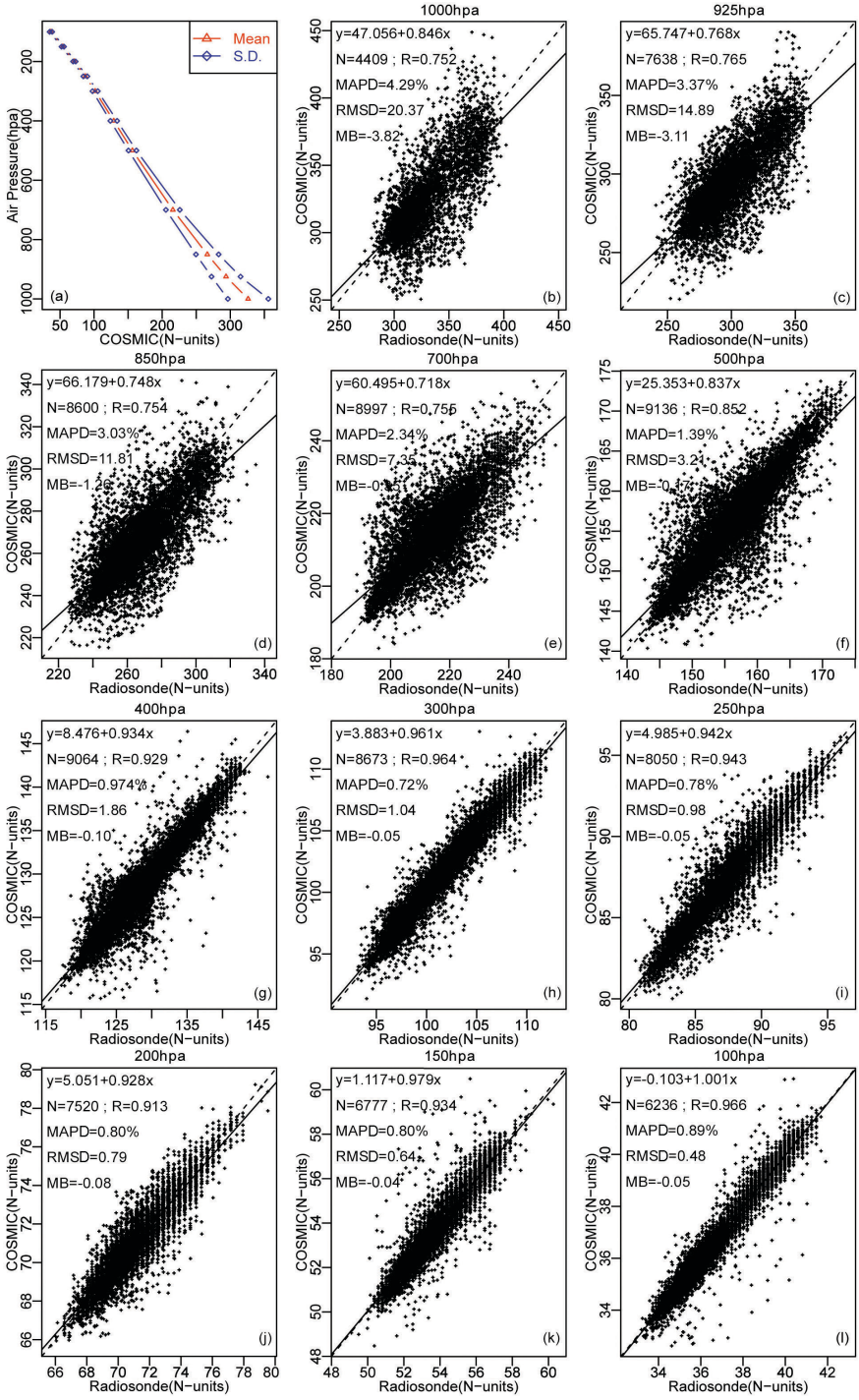

Figure 2: Scatter plots of the global COSMIC vs RS refractivity at different levels. The dashed line is the 1:1 line. The solid line is the best fit of the RO to the RS data.

3.2 Latitudinal variations of COSMIC-RS refractivity differences

We next show the COSMIC-RS refractivity differences in three latitude bands, 30°– 30°N (tropics), 30°-60° in the northern hemisphere (NH) and southern hemisphere (SH) for middle latitudes, and 60°–90° for high latitudes. The MB, RMSD and MAPD of COSMIC refractivity were calculated for the three latitude bands (Figure 3).

Figure 3*a* shows the MB at different latitudes. The absolute values of MB decrease with increasing height from 1000 to 400 hPa, and the MB is highest at –6.984 N-units in the low latitudinal tropical area, the values for the middle latitudinal area are –3.730 N-units, and the lowest is for the high latitudinal area at –1.723 N-units. This is mainly related to atmospheric humidity in the lower troposphere; the water vapor content is higher in the tropics than in the middle and high latitudes, which results in large observational errors of both COSMIC and radiosonde data. Figure 3*b* shows that the RMSD of COSMIC-RS refractivity decreases with height at all latitudes. At the levels of 1000–400 hPa, the RMSD is largest from 2.10 to 26.10 N-units at low latitudes, lower at middle latitudes from 1.85 to 19.53 N-units, and smallest at high latitudes from 1.61 to 11.00 N-units. Figure 3c shows the MAPD of COSMIC-RS refractivity at different latitudes, the MAPD decreases with increasing height, reaches the minimum at 300 hPa, and then rises slightly above 300 hPa. At the levels of 1000–400 hPa, the MAPD is largest for 1.20–5.73 % at low latitudes, smaller at middle latitudes for 0.96–4.19 %, and smallest at high latitudes for 0.79–2.39 %.

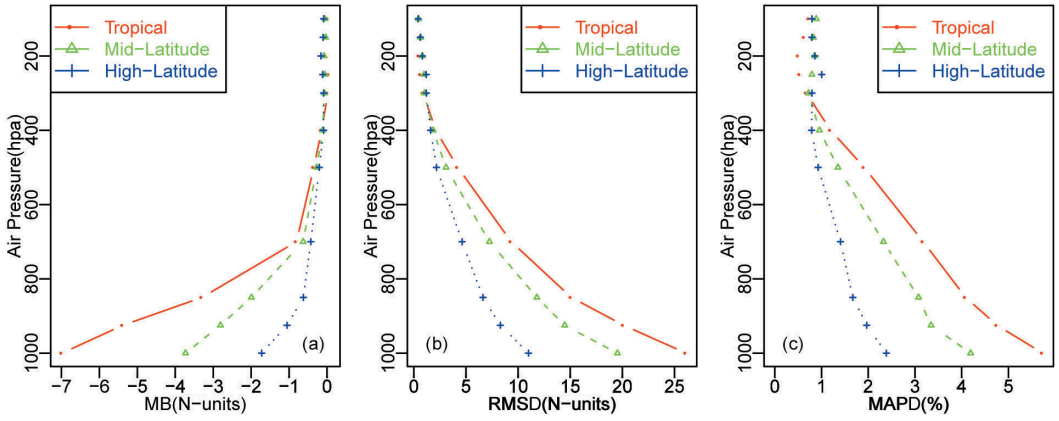

Figure 3: COSMIC-RS refractivity differences averaged over different latitude bands.

3.3 Seasonal variations of COSMIC-RS refractivity differences

In order to determine the seasonal differences between COSMIC and RS refractivity, here January in the NH and July in the SH represent winter, April in the NH and October in the SH represent spring, July in the NH and December in the SH represent summer, and October in the NH and April in the SH represent autumn. The MB, RMSD and MAPD of COSMIC-RS refractivity were calculated for the different seasons.

Figure 4 shows vertical profiles of the MB, RMSD, and MAPD statistics for the COSMIC-RS refractivity differences in the four seasons. Below 300 hPa, all three measures of differences are greatest in summer, which is expected because of the higher water vapor content in the troposphere. The negative biases are smallest in spring. The RMS differences are smallest in winter and spring while the smallest mean

absolute percentage differences occur in winter. Hence, the COSMIC-RS refractivity differences in the troposphere exhibit significant variation throughout the seasons and decrease from summer, autumn, spring, to winter. However, above 300 hPa, only small differences are observed.

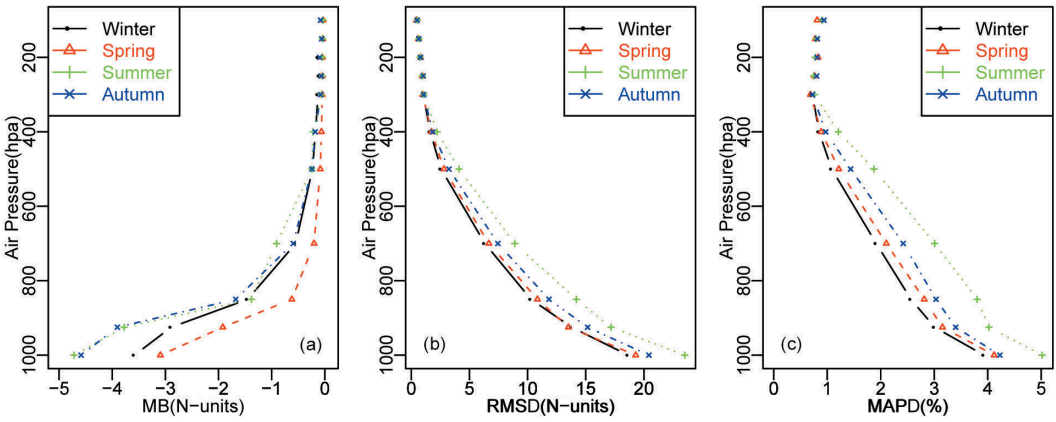

Figure 4: Vertical profile of COSMIC-RS refractivity differences in different seasons.

3.4 Spatio-temporal analysis of global COSMIC refractivity

In this section, we present the spatio-temporal analysis of global COSMIC refractivity. The COSMIC daily refractivity at 925 and 300 hPa were interpolated respectively with the cell size of 0.5° in the globe using the inverse distance weighted method, and the daily interpolated COSMIC refractivity at the two atmospheric levels in 2014 were averaged to generate global distribution maps of annual mean refractivity (Figure 5a and 5f), then the monthly mean refractivities in January, April, July and October were subtracted from the annual means, and the refractivity difference maps were drawn for four typical months (Figure 5b–5e and 5h–5j). These maps represent the global spatial patterns of COSMIC refractivity in the atmospheric boundary layer and the top of the troposphere in whole year and at different seasons.

The left panels in Figure 5 show global distribution maps of the COSMIC annual mean refractivity (5a) and the departures from the annual mean for January, April, July and October 2014 (5b, 5c, 5d and 5e) at 925 hPa. The highest refractivity ranges from 305 to 325 N-units at low latitudes, especially over the oceans; the refractivity is relatively low (275–295 N-units) in the latitudes above 30° in the NH and SH. Hence, the variability of global refractivity in the atmospheric boundary layer is mainly dominated by water vapor, and the global distribution pattern of refractivity is also in accordance with the water vapor (Barton, 2004; Chen and Liu, 2016). Due to the differences of water vapor in different seasons and latitudes and the different seasons in the NH and SH, the refractivity in January and April in the NH is lower than the annual mean value, and the maximum difference reaches –14.8 N-units, while the refractivity in the SH is higher than the annual mean value, and the maximum difference is close to 12.7 N-units. The global refractivity in July and October displays the inverse pattern, the refractivity anomalies at the latitudes for 0–60°N in the NH and 0–30°S in the SH are largest. In four representative months, the differences of refractivity in January and July are most significant while those in April and October are rather less.

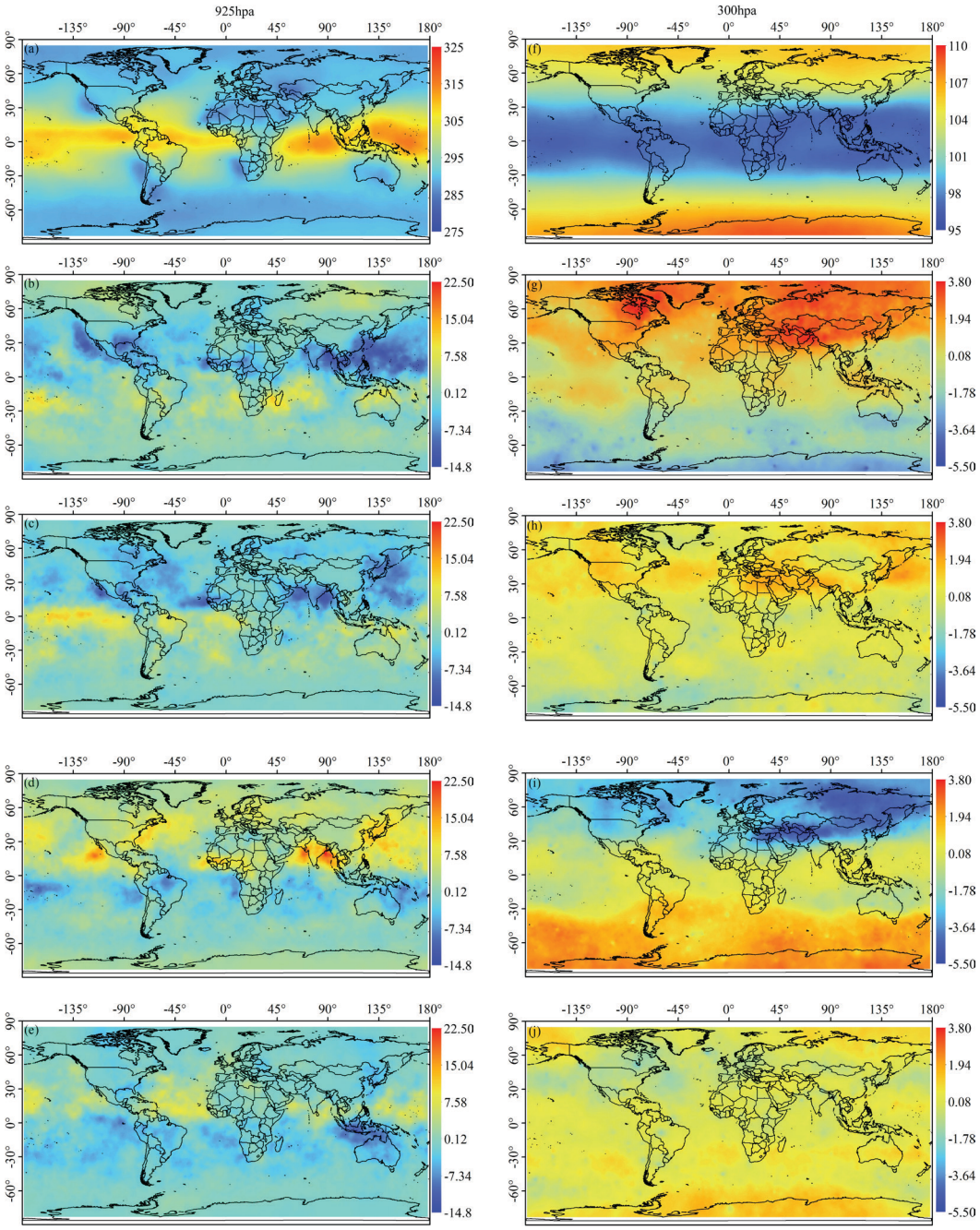

Figure 5: Global distribution maps of the COSMIC annual mean refractivity and anomalies (differences from the annual mean) in four typical months at 925 and 300 hPa (Left and right panels represent levels of 925 and 300 hPa; Row 1 is COSMIC annual mean refractivity; Rows 2–5 are the refractivity anomalies in January, April, July and October respectively.)

The right panels in Figure 5 show global distribution maps of the COSMIC mean annual refractivity

(5f) and the departures from the annual mean for January, April, July and October 2014 (5g, 5h, 5i and 5j) at 300 hPa. Since this level is in the upper the troposphere, the global refractivity is rather low (Figure 5f), and the refractivity is the smallest in the tropics at 30°S–30°N, then it increases gradually with latitude increasing in the NH and SH. At this upper tropospheric level, the water vapor pressure is small, and the refractivity is mainly determined by temperature and is inversely proportional to temperature. Since January belongs to winter in the NH and summer in the SH, and air temperature decreases as latitude increases, the refractivity in middle and high latitudes in the NH is very high. Hence there is a high positive anomaly compared with the annual mean value, and the relatively high negative bias is in middle and high latitudes in the SH. The global distribution pattern of refractivity shows an inverse pattern in July; there is a high negative anomaly in the latitudes above 30 °N in the NH and positive anomaly in latitudes above 30°S in the SH. April and October are in the transitional seasons, the refractivities in these two months are a little higher than the mean annual values, and their differences are not very large.

4 SUMMARY AND CONCLUSIONS

This study evaluated the differences of COSMIC RO-RS refractivity at different atmospheric levels, latitudes, and seasons. The temporal and global spatial distribution patterns of COSMIC refractivity were analyzed at atmospheric levels of 925 and 300 hPa. We conclude the following:

1. The COSMIC RO refractivity is in good agreement with the radiosonde refractivity at different atmospheric levels. The COSMIC-RS refractivity differences decrease with increasing height in the troposphere above 300 hPa and are very small above the tropopause.
2. The COSMIC RO-RS refractivity differences exhibit distinct latitudinal variations. At atmospheric levels above 400 hPa, the differences of COSMIC-RS refractivity are highest at low latitudes, intermediate at middle latitudes, and lowest at high latitudes, whereas the opposite is observed below 400 hPa.
3. The COSMIC RO-RS refractivity differences in the troposphere exhibit significant variation throughout the seasons and decrease from summer, autumn, spring, to winter. However, above the tropopause, only small differences are observed.
4. The global annual mean refractivity at 925 hPa is the highest in the tropics and decreases as latitude increases in the NH and SH. The variability of refractivity at this level is mainly dominated by water vapor. However, the global annual mean refractivity distribution at 300 hPa is just the opposite because the refractivity is mainly determined by temperature. Refractivity anomalies relative to the annual mean values in January and July are very significant, whereas the differences are not large in the transitional seasons of April and October.

Acknowledgments

This research was funded jointly by the construction project of weather modification in the Northwast China from China Meteorological Administration (grant number: RYSY201907), the Foundation of Key Laboratory of South China Sea Meteorological Disaster Prevention and Mitigation of Hainan Province, China (grant number: SCSF201909) and the research fund of NUIST-UoR International Research Institute (grant number: 1321041901001). The authors are very grateful to two anonymous reviewers

and the editors for their constructive and helpful suggestions. The authors thank the COSMIC Data Analysis and Archive Center (CDAAC) for the data support.

Literature and references:

Adeyemi, B. (2004). Tropospheric Radio Refractivity over Three Radiosonde Stations in Nigeria. Ife Journal of Science, 6, 167–176. DOI: https://doi.org/10.4314/ijs.v6i2.32144

Anthes, R. A. (2011). Exploring Earth's atmosphere with radio occultation: contributions to weather, climate and space weather. Atmospheric Measurement Techniques, 4, 1077–1103. DOI: https://doi.org/10.5194/amt-4-1077-2011

Anthes, R., Rieckh, T. (2018). Estimating observation and model error variances using multiple data sets. Atmospheric Measurement Techniques, 11, 4239–4260. DOI: https://doi,org/10.5194/amt-11-4239-2018

Anthes, R. A., Rocken, C., Kuo, Y.H. (2000). Applications of COSMIC to Meteorology and Climate. Terrestrial Atmospheric & Oceanic Sciences, 11 (1), 115–156. DOI: https://doi.org/10.3319/TAO.2000.11.1.115(COSMIC)

Anthes, R. A., Ector, D., Hunt, D. C., Kuo, Y. H., Rocken, C., Schreiner, W. S., Sokolovskiy, S., Syndergaard, S., Wee, T. K., Zeng, Z., Bernhardt, P. A., Dymond, K. F., Chen, Y., Liu, H., Manning, K., Randel, W. J., Trenberth, K. E., Cucurull, L., Healy, S. B., Ho, S.P., McCormick, C., Meehan, T. K., Thompson, D. C., Yen, N. L. (2008). The COSMIC/FORMOSAT-3 Mission: Early Results. Bulletin of the American Meteorological Society, 89, 313–333. DOI: https://doi.org/10.1175/BAMS-89-3-313

Ao, C. O., Meehan, T. K., Hajj, G. A., Mannucci, A. J., Beyerle, G. (2003). Lower Troposphere Refractivity Bias in GPS Occultation Retrievals. Journal Geophysical Research, 108, 4577. DOI: https://doi.org/10.1029/2002JD003216

Barton, I. J. (2004). Global water vapor analyses over the oceans using Along Track Scanning Radiometer infrared data. Journal Geophysical Research, 109, D02303. DOI: https://doi.org/10.1029/2002JD002856

Bean, B. R., Thayer, G. D. (1959). Central Radio Propagation Laboratory Experiments Reference Atmosphere. J. Research of the National Bureau of Standards D. Radio propagation. 63D, 315–317.

Bevis, M., Businger, S., Herring, T., Rocken, C., Anthes, R., Ware, R. (1992). GPS Meteorology: Remote Sensing of Atmospheric Water Vapor Using the Global Positioning System. Journal Geophysical Research, 97, 15787–15801. DOI: https://doi.org/10.1029/92JD01517

Chen, B., Liu, Z. (2016). Global water vapor variability and trend from the latest 36 year (1979 to 2014) data of ECMWF and NCEP reanalyses, radiosonde, GPS, and microwave satellite. Journal of Geophysical Research: Atmospheres, 121, 11442–11462. DOI: https://doi.org/10.1002/2016JD024917

Chen, S. Y., Huang, C. Y., Kuo, Y. H., Guo, Y. R., Sokolovskiy, S. (2009). Assimilation of GPS Refractivity from FORMOSAT-3/COSMIC Using a Nonlocal Operator with WRF 3DVAR and Its Impact on the Prediction of a Typhoon Event. Terrestrial, Atmospheric and Oceanic Sciences, 20 (1), 22, 133–154. DOI: https://doi.org/10.3319/TAO.2007.11.29.01(F3C)

Chen, S. Y., Huang, C. Y., Kuo, Y. H., Sokolovskiy S. V. (2011). Observational error estimation of FORMOSAT-3/COSMIC GPS radio occultation data. Monthly Weather Review, 139, 853–866. DOI: https://doi.org/10.1175/2010MWR3260.1

Cucurull, L., Kuo, Y. H., Barker, D., Rizvi, S. R. H. (2006). Assessing the impact of simulated cosmic GPS radio occultation data on weather analysis over the Antarctic: a case study. Monthly Weather Review, 134, 3283–3296. DOI: https://doi.org/10.1175/mwr3241.1

Fjeldbo, G., Eshleman, V. R. (1969). Atmosphere of Venus as Studied with the Mariner 5 Dual Radio-Frequency Occultation Experiment. Radio Science, 4, 879–897. DOI: https://doi.org/10.1029/RS004i010p00879

Fjeldbo, G., Kliore, G. A., Eshleman, V. R. (1971). The neutral atmosphere of Venus as studied with the Mariner V radio occultation experiments. Astronomical Journal, 76, 123–140. DOI: https://doi.org/10.1086/111096

Gilpin, S., Rieckh, T., Anthes, R. A. (2018). Reducing representativeness and sampling errors in radio occultation-radiosonde comparisons. Atmospheric Measurement Techniques, 11, 2567–2582, DOI: https://doi.org/10.5194/amt-11-2567-2018

Ha, J. H., Lim, G. H., Choi, S. J. (2014). Assimilation of GPS Radio Occultation Refractivity Data with WRF 3D VAR and Its Impact on the Prediction of a Heavy Rainfall Event. Journal of Applied Meteorology and Climatology, 53, 1381–1398. DOI: https://doi.org/10.1175/JAMC-D-13-0224.1

Hajj, G. A., Ao, C. O., Iijima, B. A., Kuang, D., Kursinski, E. R., Mannucci, A. J., Meehan, T. K., Romans, L. J., Juarez, M. T., Yunck, T. P. (2004). CHAMP and SAC-C Atmospheric Occultation Results and Intercomparisons. Journal of Geophysical Research, 109, D06109. DOI: https://doi.org/10.1029/2003jd003909

Hajj, G. A., Kursinski, E. R., Romans, L. J., Bertiger, W. I., Leroy, S. S. (2002). A Technical Description of Atmospheric Sounding by GPS Occultation. Journal of Atmospheric and Solar-Terrestrial Physics, 64, 451–469. DOI: https://doi.org/10.1016/s1364-6826(01)00114-6

Hande, L. B., Siems, S. T., Manton, M. J., Lenschow, D. H. (2015). An evaluation of COSMIC radio occultation data in the lower atmosphere over the Southern Ocean. Atmospheric Measurement Techniques, 8, 97–107. DOI: https://doi.org/10.5194/amt-8-97-2015

Hayashi, H., Furumoto, J. I., Lin, X., Tsuda, T., Shoji, Y., Aoyama, Y., Murayama, Y. (2009). Validation of Refractivity Profiles Retrieved from FORMOSAT-3/COSMIC Radio Occultation Soundings: Preliminary Results of Statistical Comparisons Utilizing Balloon-Borne Observations. Terrestrial, Atmospheric and Oceanic Sciences, 20 (1), 51–58. DOI: https://doi.org/10.3319/TAO.2008.01.21.01(F3C)

He, W., Ho, S. P., Chen, H., Zhou, X., Hunt, D., Kuo, Y. H. (2009). Assessment of radiosonde temperature measurements in the upper troposphere ad lower stratosphere using COSMIC radio occultation data. Geophysical Research Letters, 36, L17807. DOI: https://doi.org/10.1029/2009GL038712

Ho, S. P., Zhou, X., Kuo, Y. H., Hunt, D., Wang, J. (2010). Global Evaluation of Radiosonde Water Vapor Systematic Biases using GPS Radio Occultation from COSMIC and ECMWF Analysis. Remote Sensing, 2, 1320–1330. DOI: https://doi.org/10.3390/rs2051320

Ho, S. P., Peng, L., Vomel, H. (2017). Characterization of the long-term radiosonde temperature biases in the upper troposphere and lower stratosphere using

COSMIC and Metop-A/GRAS data from 2006 to 2014. Atmospheric Chemistry and Physics, 17, 4493–4511. DOI: https://doi.org/10.5194/acp-17-4493-2017

Ho, S. P., Anthes, R. A., Ao, C. O., Healy, S., Horanyi, A., Hunt, D., Mannucci, A.J., Pedatella, N., Randel, W. J., Simmons, A., Steiner, A., Xie, F., Yue, X., Zeng, Z. (2019). The COSMIC-FORMOSAT-3 radio occultation mission after 12 years: accomplishments, remaining challenges, and potential impacts of COSMIC-2. Bulletin of the American Meteorological Society, 100. https://journals.ametsoc.org/doi/pdf/ 10.1175/BAMS-D-18-0290.1

Huang, C. Y., Kuo, Y. H., Chen, S. H., Vandenberghe, F. (2005). Improvements on Typhoon Forecasts with Assimilated GPS Occultation Refractivity. Weather Forecasting, 20, 931–953. DOI: https://doi.org/10.1175/waf874.1

Jiang, C. Y., Wang, B. (2001). Atmospheric Refraction Corrections of Radio Wave Propagation for Airborne and Satellite Borne Radars. Science in China (Series E), 44, 280–290. DOI: https://doi.org/10.1007/BF02916705

Kapungu, G. P., Olaniyan, O. O., Ajayi, G. O. (1981). A Sensitive Radiosonde for Refractivity Measurements in a Tropical Environment. Journal of Physics E: Scientific Instruments, 14, 817–821. DOI: https://doi.org/10.1088/0022-3735/14/7/011

Karimian, A., Yardim, C., Gerstoft, P., Hodgkiss, W. S., Barrios, A. E. (2011). Refractivity Estimation from Sea Clutter: an Invited Review. Radio Science, 46, RS6013. DOI: https://doi.org/10.1029/2011RS004818

Kuo, Y. H., Wee, T. K., Sokolovskiy, S., Rocken, C., Schreiner, W., Hunt, D., Anthes, R. A. (2004). Inversion and error estimation of GPS radio occultation data. Journal of the Meteorological Society of Japan, 84 (1B), 507–531. DOI: https://doi.org/10.2151/jmsj.2004.507

Kuo, Y. H., Schreiner, W. S., Wang, J., Rossiter, D. L., Zhang, Y. (2005). Comparison of GPS Radio Occultation Soundings with Radiosondes. Geophysical Research Letters, 32, L05817. DOI: https://doi.org/10.1029/2004GL021443

Kuo, Y. H., Sokolovskiy, S. V., Anthes, Richard, A., Vandenberghe, F. (2000). Assimilation of GPS Radio Occultation Data for Numerical Weather Prediction. Terrestrial, Atmospheric and Oceanic Sciences, 11 (1), 157–186. DOI: https://doi.org/10.3319/tao.2000.11.1.157(cosmic)

Liao, M., Zhang, P., Yang, G. L., Bi, Y. M., Liu, Y., Bai, W. H., Meng, X. G., Du, Q. F., Sun, Y. X. (2016). Preliminary Validation of the Refractivity from the New Radio Occultation, sounder GNOS/FY-3C. Atmospheric Measurement Techniques, 9, 781–792. DOI: https://doi.org/10.5194/amt-9-781-2016

Liao, Q., Zheng, S., Shi, H. (2016). Joint Inversion of Atmospheric Refractivity Profile Based on Ground-Based GPS Phase Delay and Propagation Loss. Atmosphere, 7 (12). DOI: https://doi.org/10.3390/atmos7010012

Liu, H., Zou, X. (2003). Improvements to GPS Radio Occultation Ray-Tracing Model and Their Impacts on Assimilation of Bending Angle. Journal of Geophysical Research, 108, 4548. DOI: https://doi.org/10.1029/2002jd003160

Lohmann, M. S. (2007). Analysis of Global Positioning System (GPS) radio occultation measurement errors based on Satellite de AplicacionesCientificas-C (SAC-C) GPS radio occultation data recorded in open-loop and phase-locked-loop mode. Journal of Geophysical Research, 112 (D09115). DOI: https://doi.org/10.1029/2006JD007764

Lòpez, R., Río, V. (2018). High Temporal Resolution Refractivity Retrieval from Radar Phase Measurements. Remote Sensing, 10 (6), 896. DOI: https://doi.org/10.3390/rs10060896

Lowry, A. R., Rocken, C., Sokolovskiy, S. V., Anderson, K. D. (2002). Vertical Profiling of Atmospheric Refractivity from Ground-Based GPS. Radio Science, 37 (3). DOI: https://doi.org/10.1029/2000RS002565

Luers, J. K., Eskridge, R. E. (1998). Use of Radiosonde Temperature Data in Climate Studies. Journal of Climate, 11 (5), 1002–1019. DOI: https://doi.org/10.1175/1520-0442(1998)011<1002:UORTDI>2.0.CO,2

Phinney, R. A., Anderson, D. L. (1968). On the Radio Occultation Method for Studying Planetary Atmospheres. Journal Geophysical Research, 73 (5), 1819–1927. DOI: https://doi.org/10.1029/ja073i005p01819

Poli, P., Joiner, J., Kursinski, E. R. (2002). 1DVAR Analysis of Temperature and Humidity Using GPS Radio Occultation Refractivity Data. Journal of Geophysical Research, 107, 4448. DOI: https://doi.org/10.1029/2001JD000935

Poli, P., Moll, P., Puech, D., Rabier, F., Healy, S. B. (2009). Quality Control, Error Analysis, and Impact Assessment of FORMOSAT-3/COSMIC in Numerical Weather Prediction. Terrestrial Atmospheric & Oceanic Sciences, 20(1), 101–113.DOI: https://doi.org/10.3319/TAO.2008.01.21.02(F3C)

Rocken, C., Anthes, R., Exner, M., Hunt, D., Sokolovskiy, S., Ware, R., Gorbunov, M., Schreiner, W., Feng, D., Herman, B., Kuo, Y. H., Zou, X. (1997). Analysis and Validation of GPS/MET Data in the Neutral Atmosphere. Journal of Geophysical Research, 102 (D25), 29849–29866. DOI: https://doi.org/10.1029/97jd02400

Rocken, C., Kuo, Y. H., Schreiner, W., Hunt, D., Sokolovskiy, S., McCormick, C. (2000). COSMIC System Description. Terrestrial Atmospheric & Oceanic Sciences, 11(1), 21–52. DOI: https://doi.org/10.3319/TAO.2000.11.1.21(COSMIC)

Schreiner, W., Rocken, C., Sokolovskiy, S., Syndergaard, S., Hunt, D. C. (2007). Estimates of the Precision of GPS Radio Occultations from the COSMIC/FORMOSAT-3 Mission. Geophysical Research Letters, 34 (4). DOI: https://doi.org/10.1029/2006GL027557

Schreiner, W. S., Weiss, J. P., Anthes, R. A., Braun, J., Chu, V., Fong, J., Hunt, D., Kuo, Y. H., Meehan, T., Serafino, W., Sjoberg, J., Sokolovskiy, S., Talaat, E., Wee, T. K., Zeng, Z. (2020). COSMIC-2 radio occultation constellation: First results. Geophysical Research Letters, 47, e2019GL086841. DOI: https://doi.org/10.1029/2019GL086841

Smith, E. K., Weintraub, S. (1953). The Constants in the Equation for Atmospheric Refractive Index at Radio Frequencies. Proceedings of the IRE, 41, 1035–1037. DOI: https://doi.org/10.1109/jrproc.1953.274297

Sokolovskiy, S. (2003). Effect of Superrefraction on Inversions of Radio Occultation Signals in the Lower Troposphere. Radio Science, 38 (3). DOI: https://doi.org/10.1029/2002rs002728

Staten, P. W., Reichler, T. (2009). Apparent precision of GPS radio occultation temperatures. Geophysical Research Letters, 36, L24806. DOI: https://doi.org/10.1029/2009GL041046

Sun, B., Reale, A., Seidel, D. J., Hunt, D. C. (2010). Comparing radiosonde and COSMIC atmospheric profile data to quantify differences among radiosonde types and the effects of imperfect collocation on comparison statistics. Journal of Geophysical Research, 115, D23104. DOI: https://doi.org/10.1029/2010JD014457

Tang, W. L., Cha, H., Wei, M., Tian, B., Ren, X. C. (2019). An Atmospheric Refractivity Inversion Method Based on Deep Learning. Results in Physics, 12, 582–584. DOI: https://doi.org/10.1016/j.rinp.2018.12.014

Wang, J., Carlson, D. J., Parsons, D. B., Hock, T. F., Lauritsen, D., Cole, H. L., Beierle, K., Chamberlain, E. (2003). Performance of Operational Radiosonde Humidity Sensors in Direct Comparison with a Chilled Mirror Dew-Point Hygrometer and Its Climate Implication. Geophysical Research Letters, 30 (16), DOI: https://doi.org/10.1029/2003gl016985

Wang, J. H., Zhang, L. Y., Dai, A.G. (2005). Global Estimates of Water-Vapor-Weighted Mean Temperature of the Atmosphere for GPS Applications. Journal of Geophysical Research, 110, D21101, DOI: https://doi.org/10.1029/2005JD006215

Wang, B. R., Liu, X. Y., Wang, J. K. (2013). Assessment of COSMIC radio occultation retrieval product using global radiosonde data. Atmospheric Measurement Techniques, 6, 1073–1083. DOI: https://doi.org/10.5194/mt-6-1073/2013

Ware, R., Exner, M., Feng, D. Gorbunov, M., Hardy, K., Herman, B., Kuo, Y., Meehan, T. Melbourne, W., Rocken, C., Schreiner, W. ,Sokolovskiy, S., Solheim, F. Zou, X. Anthes, R., Businger, S., Trenberth, K. (1996). GPS Sounding of the Atmosphere from Low Earth Orbit: Preliminary Results. Bulletin of the American Meteorological Society, 77 (1), 19–40. DOI: https://doi.org/10.1175/1520-0477(1996)077<0019:GSOTAF>2.0.CO,2

Wee, T. K., Kuo,Y. H. D., Bromwich, H., Monaghan, A. J. (2008). Assimilation of GPS Radio Occultation Refractivity Data from CHAMP and SAC-C Missions over High Southern Latitudes with MM5 4DVAR. Monthly Weather Review, 136, 2923–2944. DOI: https://doi.org/10.1175/2007mwr1925.1

Wickert, J., Reigber, C., Beyerle, G., Konig, R., Marquardt, C., Schmidt, T., Grunwaldt L., Galas R., Meehan, T., Melbourne, W. G., Hocke K. (2001). Atmosphere Sounding by GPS Radio Occultation: First Results from CHAMP. Geophysical Research Letters, 28, 3263–3266. DOI: https://doi.org/10.1029/2001gl013117

Xu, X., Luo, J., Shi, C. (2009). Comparison of COSMIC Radio Occultation Refractivity Profiles with Radiosonde Measurements. Advances in Atmospheric Sciences, 26 (6), 1137–1145. DOI: https://doi.org/ 10.1007/s00376-009-8066-y

Gong S., Zhang C., Tang G., Zhang Y., J. Han (2020). Global analysis of atmospheric refractivity profiles from COSMIC GPS radio occultation soundings. Geodetski vestnik, 64 (2), 227-240.
DOI: https://doi.org/10.15292/geodetski-vestnik.2020.02.227-240

Shaoqi Gong
School of Remote Sensing and Geomatics Engineering, Nanjing University of Information Science & Technology, Nanjing, 210044, China
(Key Laboratory of South China Sea Meteorological Disaster Prevention and Mitigation of Hainan Province, Sanya, 570203, China; National Climate Center, China Meteorological Administration, Beijing, 100081, China)
e-mail: shaoqigong@163.com

*Cunjie Zhang**
National Climate Center, China Meteorological Administration, Beijing, 100081, China
(and Key laboratory for Cloud Physics of China Meteorological Administration, Beijing, 100081, China)
e-mail: zhangcj@cma.gov.cn

** Corresponding author*

*Geshi Tang**
School of Remote Sensing and Geomatics Engineering, Nanjing University of Information Science & Technology, Nanjing, 210044, China
e-mail: tanggeshi@nuist.edu.cn

Yehui Zhang
School of Hydrology and Water Resources, Nanjing University of Information Science & Technology, Nanjing, 210044, China
e-mail: zhangyehui@nuist.edu.cn

Jing Han
Key Laboratory of South China Sea Meteorological Disaster Prevention and Mitigation of Hainan Province, Sanya, 570203, China
e-mail: hanjing8361@163.com